

See discussions, stats, and author profiles for this publication at: <https://www.researchgate.net/publication/327152105>

# Machine-Learnt Turbulence Closures For Low Pressure Turbines with Unsteady Inflow Conditions

Conference Paper · August 2018

---

CITATIONS

2

READS

383

5 authors, including:



[Harshal Akolekar](#)  
University of Melbourne  
14 PUBLICATIONS 123 CITATIONS

[SEE PROFILE](#)



[Richard D. Sandberg](#)  
University of Melbourne  
224 PUBLICATIONS 3,538 CITATIONS

[SEE PROFILE](#)



[Vittorio Michelassi](#)  
Baker Hughes Incorporated  
153 PUBLICATIONS 2,133 CITATIONS

[SEE PROFILE](#)

Some of the authors of this publication are also working on these related projects:



High-fidelity simulations and data-driven turbulence model development of high-pressure turbines [View project](#)



Machine Learning Based RANS Model Development for Low Pressure Turbines [View project](#)

## **ISUAAAT15-019**

### **MACHINE-LEARNT TURBULENCE CLOSURES FOR LPTs WITH UNSTEADY INFLOW CONDITIONS**

**Harshal D. Akolekar\***  
**Richard D. Sandberg**  
**Nicholas Hutchins**

**Vittorio Michelassi**  
Baker Hughes, a GE Company,  
Florence, Italy

**Gregory Laskowski**  
General Electric Aviation,  
Lynn, USA

Department of Mechanical Engineering,  
University of Melbourne, Australia  
Email: hakolekar@student.unimelb.edu.au

#### **ABSTRACT**

*The design of low-pressure turbines (LPT) must account for the losses generated by the unsteady interaction with the upstream blade row. The estimation of such unsteady wake induced losses requires the accurate prediction of the incoming wake dynamics and decay. Machine-learnt, non-linear turbulence closures (stress-strain relationships) have therefore been developed for LPT flows with unsteady inflow conditions with an aim to enhance the wake mixing prediction for URANS calculations. Phase-lock averaged data from large eddy simulations (LES) at a realistic isentropic exit Reynolds number and two reduced frequencies have been used as a reference in order to create explicit algebraic Reynolds stress models based on gene expression programming (GEP), using three different model-generation approaches. These models have been tested in an a priori sense and have found to improve the stress-strain relationship significantly over the Boussinesq approximation. The models generated have been correlated with certain physical phenomena taking place in the LPT flow domain and have been found to offer a good prediction of the overall physics associated with wake-mixing. These models also offer a good degree of robustness across the selected reduced frequencies. This study aids blade designers in selecting the non-linear closures capable of mimicking the physical mechanisms responsible for loss generation.*

#### **INTRODUCTION**

Low-pressure turbines experience a challenging in Reynolds numbers ranging from 50,000 to 250,000 [1]. Different physical phenomena occur throughout this range of Reynolds numbers. The boundary layer on the suction side, which is largely laminar in nature, becomes prone to flow separation at moderately-low Reynolds numbers in regions of local-adverse pressure gradients. The selection of fundamental LPT design parameters, like the vane and blade count, the revolution speed, and the axial flow velocity ( $V_x$ ), concurrently determine the values of both the flow coefficient ( $\Phi$ ), and the reduced fre-

quency ( $F_{red}$ ). These two parameters control the dynamics of the periodic unsteady incoming wakes from the previous blade-rows [2], which are the dominant source of unsteady losses in LPTs. These wakes interact with and perturb the suction side boundary layer and affect the laminar separation onset, size of the separation bubble and its turbulent reattachment. Moreover, these wakes also induce other wake-wake interactions in the flow-field. A number of experimental studies [1,3–6], and high fidelity simulations [2, 7–10] have been conducted to investigate the nature and influence of these unsteady phenomenon on the performance of LPTs. All of these phenomena affect the wake-mixing in LPTs which in turn influences the losses generated and thus the net efficiency. Praisner et al. [11] suggested that the losses due to wake-mixing can contribute up to 1.5 percent of lost efficiency in LPTs.

Much of the design process for LPTs is, however, conducted using RANS based turbulence models. Accurate prediction of the wake-mixing and other complex phenomena in LPTs is still a challenge for existing RANS models as shown by a number of studies [12, 13]; and there is plenty of scope for improvement in these models. One of the reasons that RANS closures fail at predicting the turbulent wake mixing with the required degree of accuracy is the use of the Boussinesq approximation [14] for the stress-strain relationship. There are numerous approaches to address the shortcomings in this relationship, however, the most computationally efficient approach to address the shortcomings of the Boussinesq approximation are explicit algebraic Reynolds stress models (EARSM) [15]. A number of EARSMs have been developed for turbulent flows [16, 17] using analytical approaches; however, this study uses a machine-learning based approach for non-linear EARSM development to take full advantages of a set of high fidelity simulations.

Data-driven turbulence modeling is an upcoming field with great potential that has been applied to a multitude of cases using a number of methods. Duraisamy et al. [18] used non-dimensional flow variables to modify the Spalart Allmaras model using neural networks and inverse modeling. These models were used by Singh et al. [19] which showed good gen-

\*Address all correspondence to this author.

eralization capabilities for a class of flows around airfoils. Ling and Templeton [20] showed the importance of embedding tensorial invariance within machine learning approaches and used deep neural networks to improve Reynolds stress predictions for ducts. Wang et. al [21] proposed a data-driven approach to improve discrepancies in RANS modeled Reynolds stresses for two geometries: periodic hills and a square duct. However, even though they improved the Reynolds stress prediction, they could not translate this improvement to mean flow fields. This issue arose due to ill-conditioned models. Wu et al. [22] proposed a method to overcome the ill-conditioning issue, and the models that were thus developed not only brought improvement in the mean flow-field but also over different test cases. Milani et al. [23] used random forests to improve heat-flux modeling for film cooling applications.

Ferreira [24] introduced GEP which was a new adaptive algorithm for solving regression based problems. Weatheritt & Sandberg [25] developed GEP for turbulence modeling, which creates new EARSM closures imposing Galilean invariance. The algorithm not only improved the Reynolds stress prediction, but also improved the mean flow features for a few canonical cases [26]. GEP is relatively inexpensive as compared to other machine learning techniques used for previous turbulence model studies and the models generated via this method have an added advantage that they do not require any supporting machine-learning or high fidelity databases for their implementation into CFD codes. GEP was applied for the first time on a turbomachinery component when an *a priori* study was conducted for high pressure turbines [27]. The EARSMs developed showed significant improvement over the baseline case. However, these models were not implemented into (U)RANS calculations. Akolekar et al. [28] not only developed a family of EARSMs for LPT flows with steady inflow conditions but also implemented them into URANS calculations and tested them across two topologically different flows in order to enhance wake-mixing prediction. The models not only offered significant improvements in terms of secondary statistics, but also improved mean flow features such as velocity, loss profiles and wake maturity, etc. These models demonstrated a good degree of robustness across the two cases tested. A similar study was conducted by Sandberg et al. [29] for a trailing edge slot, using GEP to enhance heat flux modeling across two lip thickness ratios.

This study aims to extend the analysis conducted by Akolekar et al. [28] to LPTs with unsteady inflow conditions; developing a framework, that, for the first time will produce EARSMs which enhance the wake mixing prediction of these cases. LES data for two cases with an isentropic exit Reynolds number of 100,000 and reduced frequencies of 0.624 and 1.866 have been used as reference data for model generation. Using the phase-lock averaged and time-averaged data that is available, three different approaches have been used to develop a large family of models. The detailed assessment and performance in the *a priori* sense of the models that are developed from each of these approaches forms the majority of this study. An extensive discussion about the correlation of the model coefficients with physical phenomena has also been addressed.

After a robustness study of these models across the different phases and cases, a few models have been selected for conducting future URANS calculations. It is expected that this study offers blade designers an additional insight into the kinds of linear and non-linear stress-strain relationships (EARSMs) that are required to improve the accuracy of existing (U)RANS modeling techniques for LPTs with unsteady inflow conditions.

## NOMENCLATURE

|                  |  |
|------------------|--|
| $a_{ij}$         | Normalized anisotropy tensor   |
| $C$              | Blade chord length   |
| $F_{red}$        | Reduced frequency  |
| $I_k$            | Scalar invariant   |
| $J$              | GEP cost function  |
| $J\%$            | Percentage error reduction   |
| $k$              | Turbulent kinetic energy   |
| $p$              | Phase number   |
| $P_{bar}$        | Bar pitch  |
| $P_{TKE}$        | TKE production   |
| $Re_{2is}$       | Isentropic exit Reynolds number  |
| $S_{ij}$         | Strain rate: $\frac{1}{2}(\partial_{x_j} U_i + \partial_{x_i} U_j)$          |
| $S'_{ij}$        | Deviatoric component of strain rate: $S_{ij} - \frac{1}{3}\delta_{ij}S_{kk}$ |
| $t$              | Time   |
| $T$              | Time period  |
| $U$              | Bar tangential speed   |
| $\overline{v_2}$ | Wall-normal turbulent velocity fluctuations                                  |
| $V_2$            | Exit absolute flow velocity  |
| $V_{ij}^k$       | Tensor basis function  |
| $V_x$            | Axial velocity   |
| $\mu_t$          | Eddy viscosity   |
| $\rho$           | Density  |
| $\tau$           | Turbulent time scale: $(1/\omega)$   |
| $\tau_{ij}$      | Reynolds stress tensor: $\rho \overline{u'_i u'_j}$                          |
| $\Phi$           | Flow coefficient   |
| $\omega$         | Specific dissipation rate  |
| $\Omega_{ij}$    | Rotation rate tensor: $\frac{1}{2}(\partial_{x_j} U_i - \partial_{x_i} U_j)$ |

## ACRONYMS

|         |  |
|---------|--|
| B       | Boussinesq                               |
| LES     | Large Eddy Simulation                    |
| EARSM   | Explicit Algebraic Reynolds Stress Model |
| GEP     | Gene Expression Programming              |
| LPT     | Low-Pressure Turbine                     |
| Mod-PA  | Models based on individual phases        |
| Mod-Phy | Models based on physics                  |
| Mod-TA  | Models based on the time averaged flow   |
| RANS    | Reynolds Averaged Navier–Stokes          |
| TE      | Trailing Edge                            |
| TKE     | Turbulent Kinetic Energy                 |

## EARSMs for TURBULENCE MODELS

The Boussinesq approximation, which is one of the major sources of error in RANS modeling, can be broken up into the sum of isotropic and anisotropic contributions

$$\tau_{ij} = \underbrace{\frac{2}{3}\rho k \delta_{ij}}_{\text{isotropic}} - \underbrace{2\mu_t \left( S_{ij} - \frac{1}{3}\frac{\partial u_k}{\partial x_k} \delta_{ij} \right)}_{\text{anisotropic}}. \quad (1)$$

Of the many of ways to address the deficiencies of the Boussinesq stress-strain relation, EARSMs are an effective and computationally efficient approach. Beginning from the weak equilibrium hypothesis [30], a class of turbulence closures, known as EARSMs [15] were developed to express the anisotropy tensor  $a_{ij}$  as a function of a tensor basis  $V_{ij}^k$  and scalar invariants  $I_k$ . These models add non-linear terms to the stress-strain relationship and their calculation incurs little computational expense. Equation (2) defines  $a_{ij}$ , which is normalized by  $2\rho k$ , for both the Boussinesq approximation and EARSMs

$$a_{ij} \equiv \frac{\tau_{ij}}{2\rho k} - \frac{1}{3} \delta_{ij}, \quad (2a)$$

$$a_{ij}^B = -\frac{v_t}{k} S'_{ij} \quad (\text{Boussinesq}), \quad (2b)$$

$$a_{ij}^{\text{EARSM}} = -\frac{v_t}{k} S'_{ij} + f(V_{ij}^1, V_{ij}^2, V_{ij}^3, \dots, I_1, I_2, \dots). \quad (2c)$$

Note that the  $-\frac{v_t}{k} S'_{ij}$  term is maintained in the anisotropy relation in Eq. (2c) for the EARSM model in order to maintain numerical stability when these models are implemented into (U)RANS solvers. The tensor basis and set of scalar invariants, used to define  $a_{ij}^{\text{EARSM}}$ , are functions of the non-dimensional strain and rotation rate tensors, denoted by  $s_{ij} = \tau S'_{ij}$  and  $w_{ij} = \tau \Omega_{ij}$ ; where  $\tau$  is the time scale denoted by  $1/\omega$ . For the flow scenario considered in this work, only the basis functions up to the second order have been considered. The selected basis functions and invariants are:

$$V_{ij}^1 = s_{ij}, \quad V_{ij}^2 = s_{ik}w_{kj} - w_{ik}s_{kj}, \quad (3a)$$

$$V_{ij}^3 = s_{ik}s_{kj} - \frac{1}{3} \delta_{ij} s_{mn} s_{nm}, \quad (3b)$$

$$V_{ij}^4 = w_{ik}w_{kj} - \frac{1}{3} \delta_{ij} w_{mn} w_{nm}, \quad (3c)$$

$$I_1 = s_{mn} s_{nm}, \quad I_2 = w_{mn} w_{nm}. \quad (3d)$$

The data used for model development in this study has been spanwise averaged. This averaging sets the shear components (other than  $\tau_{xy}$ ) of the Reynolds stress to zero. However, the normal component of the Reynolds stress in the third direction ( $\tau_{zz}$ ) does continue to exist. For EARSMs developed for statistically 2D flows in the past [17] only the first three basis functions from Eq. (3) have been used. However, in this study the 4<sup>th</sup> basis function (which is the last quadratic tensor basis function) has also been used as it is non-zero due to the presence of  $\tau_{zz}$ . Other basis functions have not been used, as it has been found that the contribution of these higher order tensor basis functions is negligible to the reduction of mean square error.

## LES FLOW CONFIGURATION

A number of LES were carried out by Michelassi et al. [2] for a T106A LPT blade, which has a pitch to chord ratio of 0.799 and real chord of 0.1m. It is these datasets that have been used for the EARSM development outlined in this work. The LES have been shown to agree well with data from DNS [7], which in turn were shown to reproduce experimental results

**Table 1:** List of LES configurations.

| Case | # Bars | Blade pitch | Bar pitch | Bar speed | $\Phi$ | $F_{red}$ |
|------|--------|-------------|-----------|-----------|--------|-----------|
| 1B2U | 1      | 0.799       | 0.799     | 0.820     | 0.850  | 0.624     |
| 2B3U | 2      | 0.799       | 0.400     | 1.230     | 0.569  | 1.866     |

[31]. The reference isentropic exit Reynolds number ( $Re_{2is}$ ) is 100,000 and the flow coefficient and reduced frequencies have been varied over certain ranges in order to offer a broad spectrum of qualitative information for the blade designer. In order to develop unsteady inflow for the LPT, moving cylindrical bars (with a non-dimensional speed of 0.41) were used 70% real chord upstream of the blade leading edge. For the purpose of model development, two cases have been selected that show different flow features, which are abbreviated as 1B2U and 2B3U. A detailed description of these two cases is given in Table 1. The blade and bar pitch are normalized with respect to the real chord. In a linear cascade with moving upstream bars the reduced frequency and the flow coefficient are defined as:

$$F_{red} = \frac{U}{P_{bar}} \frac{C}{V_2}, \quad \Phi = \frac{V_x}{U}. \quad (4)$$

Each case is referred to by its bar count and speed (i.e. 1B2U corresponds to 1 bar per blade pitch and nominal bar speed of 0.82). An effective way to show how the combination of  $F_{red}$  and  $\Phi$  affects the incoming wake dynamics is to plot phase-lock averaged snapshots of the turbulent kinetic energy (TKE), as this traces the path of the wake to the blade leading edge, into the passage and to the trailing edge. Figure 1 depicts the

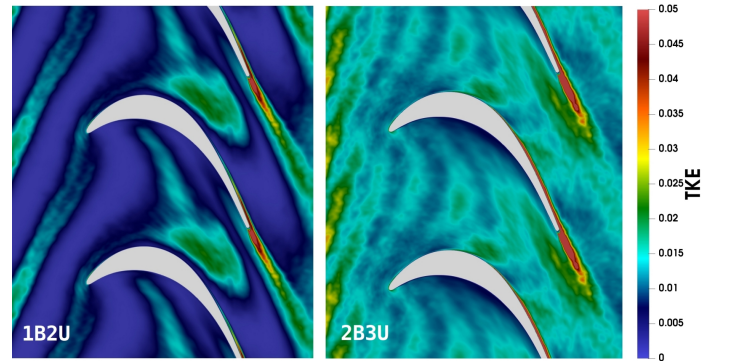


**Figure 1:** Phase-lock averaged TKE snapshots for the 1B2U and 2B3U cases.

TKE for phase-lock averaged flow fields of the 1B2U and 2B3U cases. One stark difference between the two cases is that there are discrete incoming wakes in the 1B2U case whereas in the 2B3U case, the wakes seem to merge with one another; also known as ‘fogging’. The discrete unsteadiness that is exhibited by the 1B2U case seems to fade away as the bar speed and bar pitch are increased (2B3U), which leads to more pronounced wake-wake interaction at the inlet. The 2B3U case, in a limiting condition, represents a case of plain free-stream turbulence, as

the discrete wakes start to merge. In order to receive insights for the EARSM development process across a wide range of flow conditions, both of these cases have been selected. The EARSM development uses phase-lock averaged data sets; at 20 and 17 equispaced phase angles for the 1B2U and 2B3U cases respectively, over one incoming wake passing period ( $T$ ). There are two ways of identifying particular phase-lock average flow fields; one of them simply refers to it by the phase number (i.e. phase 5 as p5); the other represents the data across one time period ( $T$ ). A simple conversion can be made between the time ( $t$ ) and the phase number as follows:  $t/T = p/N$ , where  $N=20$  &  $N=17$  for the 1B2U and 2B3U cases respectively. The next section outlines the methodology for EARSM development.

## MACHINE LEARNING METHODOLOGY

The EARSM development for LPTs with unsteady inflow conditions is carried out with GEP [24, 25]. Each of the phase-lock averaged datasets, for both the 1B2U and 2B3U cases, has been used as reference data to create EARSMs. The EARSM development approach is outlined in Fig. 2. As the focus of this work is to improve the wake-mixing prediction, the Reynolds stresses (or indirectly the anisotropy field:  $a_{ij}^{LES}$ , calculated from Eq. (2a)), velocity, temperature, TKE and density from a wake region are extracted from the LES and fed into the GEP algorithm. This data is also used to solve the  $\bar{v}_2$  and  $\omega$  equations of the  $k\bar{v}_2\omega$  turbulence model [32] using the so-called

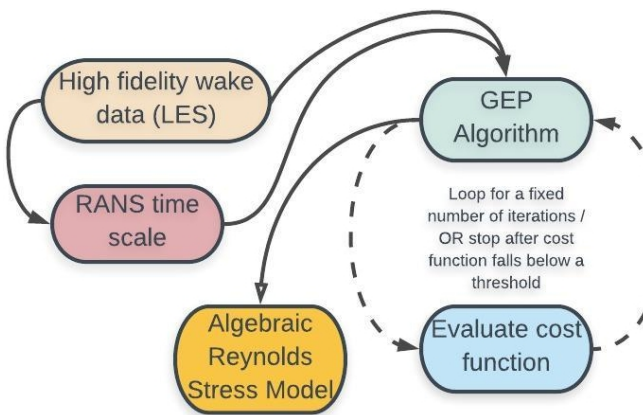


**Figure 2:** GEP algorithm at a glance.

'frozen' approach [33]. The  $k\bar{v}_2\omega$  model has been used as it was found in our numerical setup to offer the best prediction of the boundary layer and wake losses as compared to other turbulence models for LPTs [28]. The above approach allows the extraction of a relevant time scale ( $1/\omega$ ) to normalize the tensor basis functions in Eq. (3). Theoretically, it is possible to extract a dissipation ( $\omega$ ) value from the LES data; however, it has been found that this value does not in any way resemble the  $\omega$  definition used in a (U)RANS context. The value of  $\omega$  is extensively modeled for RANS calculations, which causes this value to differ significantly from values extracted directly from high fidelity simulations. The strain-rate and rotation-rate tensors are calculated using LES data and are normalized with the

RANS time scale. Using these normalized tensor basis functions the GEP algorithm creates a family of models which are then evaluated against a cost function. GEP, a regression based algorithm, aims to minimize the sum of the difference between the individual components of the anisotropy tensors, i.e. the anisotropy tensor that is created from the EARSMs ( $a_{ij}^{EARSM}$ ) and the one from the LES flow field ( $a_{ij}^{LES}$ ), as

$$J(a_{ij}^{EARSM}) = \frac{1}{M} \sum_{m=1}^M \sum_{i=1}^3 \sum_{j \leq i} (|a_{ij}^{LES} - a_{ij}^{EARSM}|)^2, \quad (5)$$

where  $M$  is the total number of points in the training region. As this is an iterative process, the evolution of models keeps on going for a fixed number of iterations or until the cost function falls below a certain threshold. The GEP algorithm then returns an anisotropy tensor ( $a_{ij}^{EARSM}$ ), which best fits the  $a_{ij}^{LES}$  tensor. Regression for the anisotropy tensor is sought, as it has been shown that improvements in the RANS wake-mixing prediction can be brought about by a better representation of the anisotropy tensor [28]. The anisotropy tensor also appears both in the momentum diffusion and in the TKE and  $\omega$  production terms. If the modeling for this term is improved, there will be better prediction of the wake diffusion and TKE production; which will lead to enhanced wake-mixing.

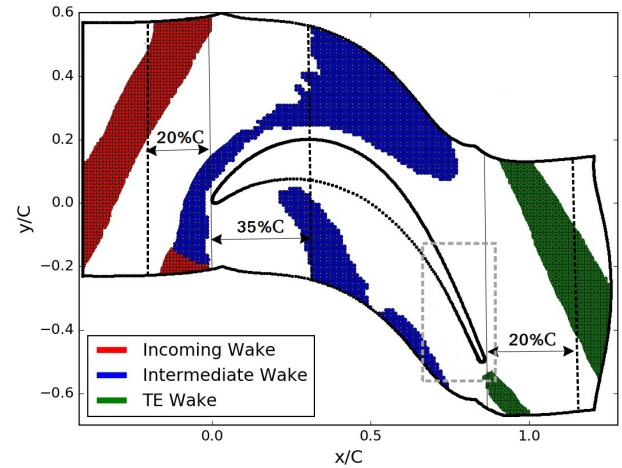


**Figure 3:** Training regions for EARSM development for phase 1 of the 1B2U case.

Since the GEP algorithm is non-deterministic in nature, it is highly likely that the algorithm will produce different coefficients for each of the basis functions every time it is executed, which leads to slightly different levels of fitness. In order to account for this slight variation, every model presented in this work is the result of running the GEP algorithm 25 times on that particular case and training region. The 25 models are then ensemble-averaged.

It was found by Akolekar et al. [28] that selecting the appropriate data or training region to improve the wake-mixing is particularly important. They showed that it is necessary to select the data in the wake region (which can be demarcated by values of TKE above a certain threshold), rather than a region

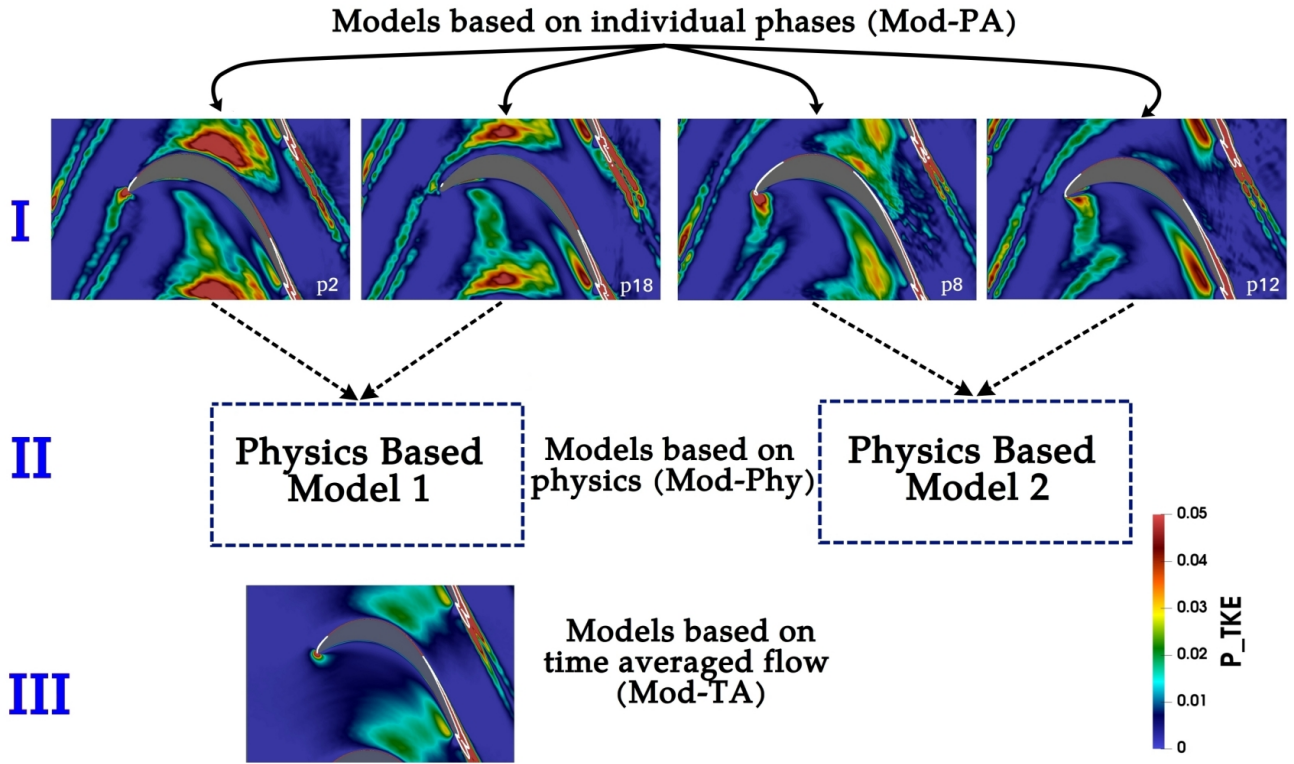


**Figure 4:** The three approaches used for EARSM development. Contour plots of TKE production for various phases and the time-averaged flow fields are shown for the 1B2U case.

which encompasses the wake and the wake passage. However, in their study only the wake coming off the blade trailing edge was considered for model development. In this study, models also need to be developed for the wakes which are incident on the leading edge of the blade and transported through the blade passage, in order to enhance the overall wake mixing in the presence of static pressure gradients. In order to effectively develop EARSMs for these wakes, the magnitudes of the tensor basis functions and scalar invariants have to be assessed in the various wake regions. They are found to differ, broadly with the region in the flow-field. Figure 3 shows three different kinds of wake regions (for phase 1 of the 1B2U case), which are each dominated by different physical phenomena. The wakes which are incoming from the previous blade row tend to be diffusion dominated whereas the wake in the blade passage (intermediate wake) undergo dilation-distortion and interact with the suction and pressure side boundary layers. The wakes coming off the blade trailing edge (TE Wake) are dominated by either higher diffusion due to the formation of Kelvin-Helmholtz roll-up vortices or non-linear phenomena due to intermediate wake and TE wake interactions. As noted by Lumley [34], it is challenging to develop a constitutive law that holds valid in regions with very different combinations of time and length scales. Therefore, it has been hypothesized that different EARSMs need to be produced for these three different regions and different model development approaches need to be compared.

Firstly, criteria need to be determined that allow objective separation of the different wake regions for which models will be trained. Analyzing the flow fields shows that there is a sharp increase in the strain rate magnitude due to the curvature ef-

fects of the LPT blade, approximately 5-7% chord upstream of the blade trailing edge. This criterion can be used to mark the inception of the intermediate wake region and was inspired by a study conducted by Michelassi and Wissink [35]. They showed that the wake (Intermediate wake in Fig. 3), when being swallowed into the blade passage, undergoes distortion and it responds to the alignment or misalignment of the strain rate tensor with the Reynolds stress tensor. The trailing edge region can be easily identified due to higher TKE values and dissipation rates as compared to the surrounding wake-passage. The near wake-region (up to 5%C in the streamwise direction from the TE of the blade) has been ignored from the TE wake training region as it drastically affects the nature of the trained models due to the high shear as compared to the rest of the (far) wake.

Using the above 2 cases, with their respective phase-lock averaged flow fields, three kinds of model types have been developed as shown in Fig. 4. In Fig. 4, contours of TKE production are shown only for four phases of the 1B2U case and for the time-averaged flow field. There is an additional contour line shown in white for  $P_{TKE} = 0.25$ , which highlights the extent of laminar separation and its effect in the TE wake. The first model type uses the individual phase-lock averaged (Mod-PA) flow fields to generate models for each individual phase and training region. As there are three training regions, this implies that there will be 60 different models (post-ensemble averaging) for the 1B2U case (i.e. the GEP algorithm was run a total 1500 times in order to obtain the 60 models for 1B2U and it was run 1275 times to obtain 51 models for the 2B3U case). In order to assess whether a large number of models are

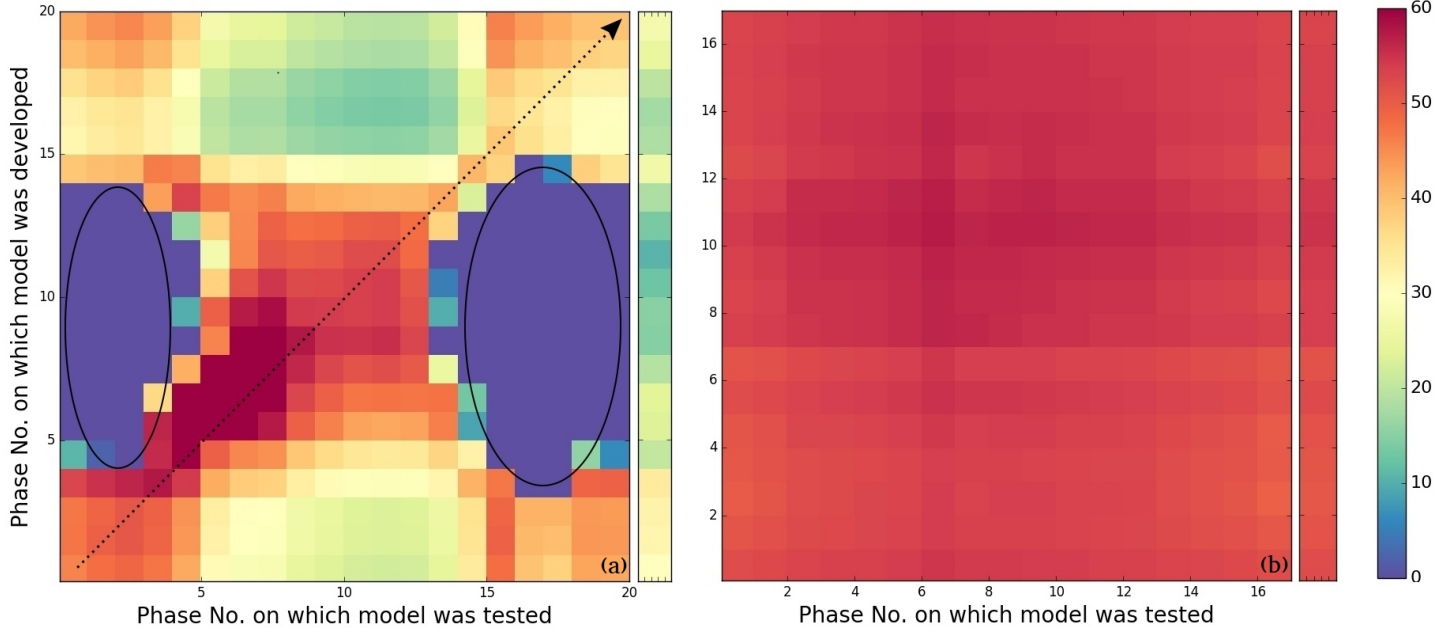


**Figure 5:** Percentage reduction in normalized mean square error ( $J\%$ ) over the Boussinesq approximation, when models developed on the TE wake region of a particular phase are tested on the TE wake region of all the phases for the (a) 1B2U and (b) 2B3U cases.

required to be developed or not to predict the physics across all the phases and training regions, alternative methods which lead to a smaller number of models have been investigated. The second type of models are ones that are based on the wake-physics (Mod-Phy). In Fig. 4, as an example, data from phases 2 & 18, along with a number of other phases (not shown here), which have similar physics, are combined together to form a larger dataset which is used for developing an EARSM. In this case, phases 8 & 12 have different trailing edge wake physics as compared to the phases 2 & 18 and hence the data from phases 8 & 12, along with a number of other phases not shown here, are used to develop a different EARSM. The criteria for the development of Mod-Phy models is discussed in later sections. The third model type uses the time-averaged statistics (Mod-TA) across one time period (i.e no phase data), similar to what was done for the cases with steady inflow conditions considered in Akolekar et al. [28], for EARSM development.

## MODELS BASED ON INDIVIDUAL PHASES

This section discusses the models that have been generated using the Mod-PA approach. These models were developed for all three wake regions for both cases. However, it was found that the models developed in the TE wake region offer the most interesting trends and correlations to flow physics, and thus have been discussed in detail. The performance of these models has been conducted in an *a priori* sense (without running any (U)RANS calculations). This will give the designer some insights into how various models perform in the different flow regimes and what are the best practices for model generation and selection.

### Error Matrices

With the Mod-PA approach for model development, each model that is generated has been tested on each of the other phases for the respective training region. This will provide in-

sight regarding onto the robustness of the models developed for each of the phases (i.e. do models trained on one particular phase perform well on the other phases). In order to achieve this, the normalized mean square error (Eq. (5)) was calculated by testing each of the models developed (20 in the case of 1B2U and 17 in the case of 2B3U) by the Mod-PA approach on each of the phase-lock averaged data sets for the respective training regions and cases. The normalized mean square errors using the Boussinesq approximation were also calculated (replace  $a_{ij}^{EARSM}$  in Eq. (5) with  $a_{ij}^B$ ). The percentage difference (i.e.  $J\% = \frac{(J^B - J^{EARSM})}{J^B} \times 100$ ) or percentage error reduction between these two normalized mean square errors for the TE wake region has been plotted in Fig. 5 for both cases. The extra column on the right of these matrices depicts the average percentage error reduction a model can bring if it is applied to all the phases.

In Fig. 5(a) (1B2U case), there are two distinct blue patches (demarcated by the ellipses) which represent either a zero or negative (which is also shown as zero for the ease of presentation) percentage reduction in normalized mean square error ( $J\%$ ) over the Boussinesq approximation. This implies that certain models, when used on other phases, do not improve the anisotropy prediction, but can in fact even worsen it. Broadly categorizing, models developed on phases 5-14 do not enhance performance when they are tested on phases 1-4 and 15-20. Models trained on phases 1-4 and 15-20, however, on the other hand, not only do offer significant percentage error reductions if they are tested on phases 1-4 and 15-20, but also offer some degree of error reduction for phases 5-14. Models trained on phases 5-14, when tested on phases 5-14 do offer a percentage error reduction of an average value of approximately 53%. Models developed on the respective phases of the TE wake region in the 2B3U case (Fig. 5 (b)), when tested on the other phases, offer a uniformly distributed percentage error

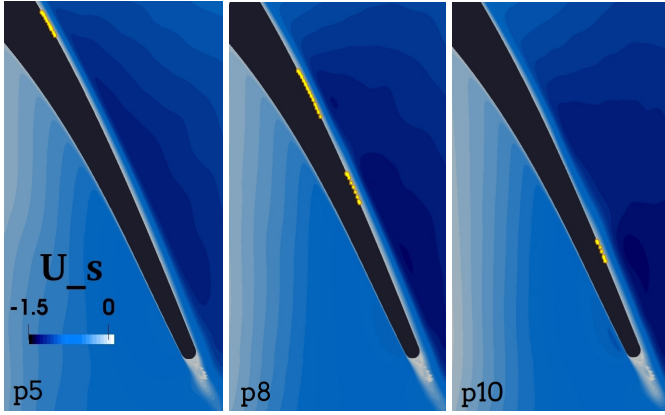


**Figure 6:** Contour plots of the streamwise velocity, highlighting the propagation of the short laminar separation bubble(s) (shown in yellow) on the suction side, for phases 5, 8 and 10 of the 1B2U case.

reduction of 55% across all the phases. These observations can be explained if the physics of the boundary layer is analyzed.

### Boundary Layer Physics

The incident wakes from previous blade rows interact with the suction side boundary layer in a number of ways. At moderate Reynolds numbers (inc.  $Re_{2is} = 100,000$ ) and mild adverse pressure gradients, there is a possibility that laminar separation can occur on the blade suction side, which in fact happens in the 1B2U case. Based on the LES data [2] of the 1B2U case, it is observed that intermittent laminar separation (short laminar separation bubbles [36]) followed by turbulent reattachment takes place. Due to the discrete incident wakes, in the 1B2U case, the shear layer on the aft-side of the suction side gets perturbed and separates. Due to these perturbations, Kelvin-Helmholtz roll-up vortices are [4, 37] formed. These roll-up vortices perturb the boundary layer further downstream which leads to the formation of more vortices; eventually breaking down into turbulence, and thereby causing boundary layer transition. A calmed region soon follows once the roll-up vortices and turbulent boundary layer has subsided. Figure 4 shows the TKE production contours for phases (2 & 18) which have calmed boundary layers and phases (8 & 12) where the Kelvin-Helmholtz roll-up vortices are shed.

Figure 6 depicts a contour plots of the streamwise velocity, which highlights the propagation of short laminar separation bubbles along the suction side boundary layer of the 1B2U case for phases 5, 8 and 10. Regions where the wall shear stress is less than zero (laminar separation) are shown by the yellow lines on the blade. The location of the above plots with respect to the LPT domain is shown by the grey box in Fig. 3. The separation bubble first appears in phase 5, and is also visible in phases 6-10. Due to the laminar separation, and boundary layer transition resulting in turbulent reattachment, there is an increase of turbulent diffusion in the boundary layer and thus in the TE wake region. Turbulence models using the Boussinesq approximation, generally cannot predict this change of diffusion across the various phases. However, when EARSMs were developed for the TE wake region, this increase in turbulent diffusion has been successfully captured in the TE wake re-

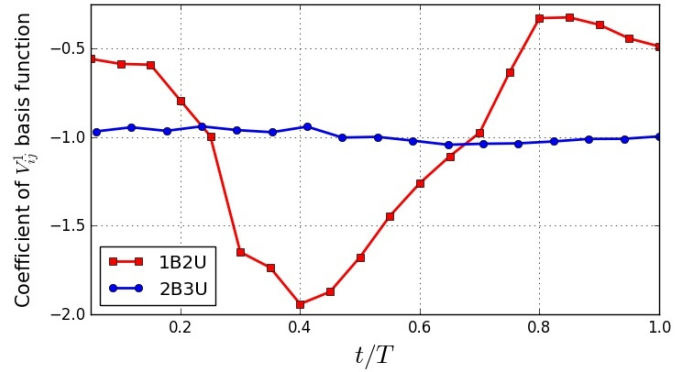


**Figure 7:** Additional diffusion (coefficient of  $V_{ij}^1$  in  $a_{ij}^{EARSM}$ ) required in the TE wake region of the 1B2U and 2B3U cases as predicted by the EARSM models, shown for one time period.

gion. The amount of additional diffusion required to predict the flow physics more accurately in each of the 20 phases is shown in Fig. 7 for both cases and for one time period. The additional diffusion is represented by the coefficient of the  $V_{ij}$  tensor basis which is in addition to that which the Boussinesq approximation already offers, from the  $-\frac{V_L}{k} S_{ij}$  term. In this plot (and also Fig. 10) models have been tested on the same phase that they were developed on (i.e. along the diagonal line in Fig. 5(a)). Note that data is available only at the markers, since only phase-lock averaged data is used. Lines between the markers are there to aid visual representation.

From Fig. 7 it is clear that additional diffusion is required for all phases to obtain significant error reduction over the Boussinesq approximation. In the 1B2U case, phases 6-12 have an additional diffusion coefficient with a magnitude greater than 1.3, as the boundary layer and TE wake region are perturbed by the laminar separation. Since the effect of the laminar separation is convected at a speed of 50-90% of the so-called freestream fluid [37], there is a sharp increase in the additional diffusion coefficient only in phase 6, even though the laminar separation bubble is visible in phase 5. The magnitude of the coefficient of the  $V_{ij}^1$  basis function gradually starts to fall from phase 8 and makes a sharp drop after phase 14, when the residual effects of the separation and perturbed boundary layer have completely subsided. A relatively calm period follows this and the boundary layer remains laminar until phase 3 of the next time period; hence the lower additional diffusion coefficient. Some instabilities start to form again in phase 4. Since the additional diffusion coefficient changes drastically between the calm phases and when there is laminar separation, distinctive blue patches are formed in Fig. 5(a), when models with higher additional diffusion coefficients are tested on models with lower additional diffusion coefficients. If models developed on phases which have lower additional diffusion (phases 1-4 & 15-20) are tested on phases with higher additional diffusion (5-14), they still reduce the error as they contribute to a fraction of the additional diffusion coefficient required to bring about the maximum possible error reduction. In the 2B3U case, due to the higher number of bar wakes and bar convection velocity, there are no discrete wakes that are being formed.

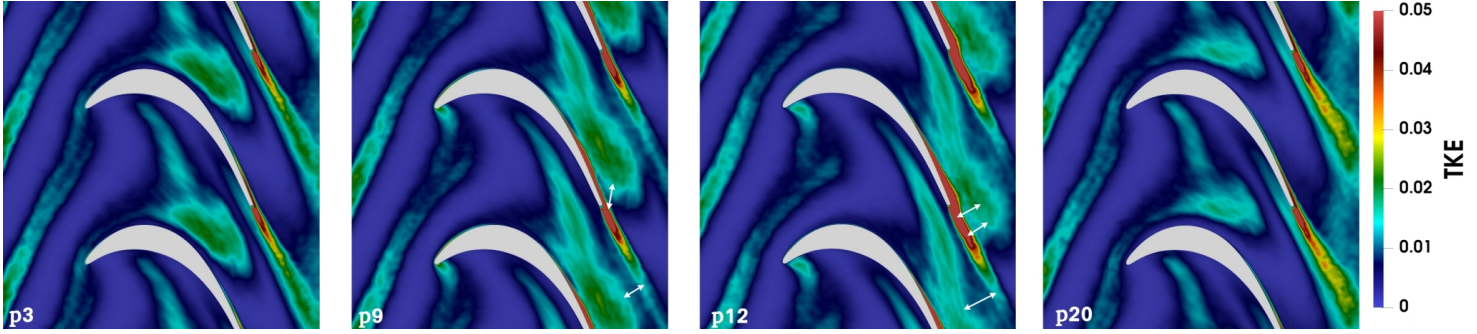


**Figure 8:** Phase-lock averaged TKE contour plots highlighting the movement of the intermediate wakes through the blade passage and their interaction, shown by the white arrows, with the TE profile wakes, for the 1B2U case.

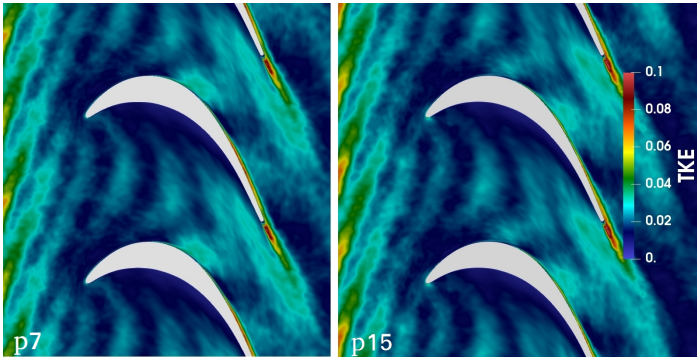


**Figure 9:** Phase-lock averaged TKE contour plots for the 2B3U case.

Consequently, the boundary layer does not have an opportunity to undergo laminar separation. Therefore, there is hardly any change in the additional diffusion coefficient across phases. Due to the higher convection speed of the incoming wakes, an additional diffusion coefficient of around -1 is still required to attain the maximum possible error reduction as outlined in Fig. 5(b). This also suggests that one EARSM is sufficient to model all the phases with a good degree of accuracy for this case.

### Intermediate Wake – TE Wake Interactions

Another interesting point to note is the percentage contribution of the non-linear terms (i.e. tensor basis  $V_{ij}^2$ ,  $V_{ij}^3$  and  $V_{ij}^4$ ) to the error reduction for the TE wake. Figure 10 demonstrates the percentage contribution of non-linear terms to the percentage error reduction when a model developed on a particular phase is tested on that same phase (i.e. along the diagonal line in Fig. 5(a)). In the 1B2U case, for phases 1-8, the contribution of the non-linear terms is less than 10%, which implies that the TE wake is diffusion dominated. From phases 9 to 16 there is an increase in the contribution of the non-linear terms to the total error reduction. This contribution can be attributed to the wake, that was originally in the intermediate region, moving downstream and interacting with the wake in the TE region. Figure 8 shows TKE contour plots of phase-lock averaged flow fields for phases 3, 9, 12 and 20 for the 1B2U case. In phase 3, the intermediate wake in the blade passage does not interact with the TE wake region; hence the very low contribution of the non-linear terms to the error reduction. The intermediate wake – TE wake interactions start to intensify in phase

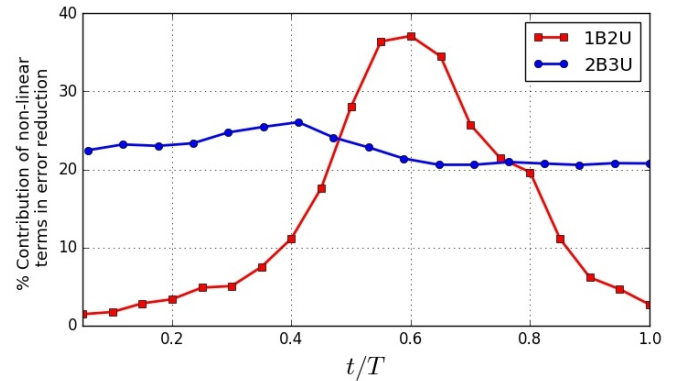


**Figure 10:** Percentage contribution of non-linear terms to the percentage normalized mean square error reduction ( $J\%$ ) for the 1B2U and 2B3U cases in the TE wake region for one time period.

9 and peak in phase 12. By phase 18, as the wake through the passage exits the domain, the effect of these interactions largely subsides, as is clearly visible from the TKE plot for phase 20. Figure 9 shows the TKE contour plots for phases 7 and 15 for the 2B3U case. Note the different scaling used for the TKE contours (to highlight the wakes for this case). In the 2B3U case, since there are no discrete wakes that propagate through the blade passage, and since there is a near continuous wake-wake interaction, the contribution of the non-linear terms remains reasonably constant. This phenomena is not only observed with the intermediate-TE wake interactions, but also in the incoming wake region of the 2B3U case. The percentage contribution of the non-linear basis functions to the percentage reduction in the normalized mean square error ( $J\%$ ) is much higher in the 2B3U case than the 1B2U case in the incoming wake region (Fig. 3), which can be attributed to stronger wake-wake interactions the 2B3U case has in this region.

### MODELS BASED ON PHYSICS & TIME AVERAGES

From the perspective of a designer, it is not convenient to run different models for each of the phases. Therefore, the performance of models of Mod-Phy and Mod-TA types (Fig. 4) have been assessed with respect to the Mod-PA approach. In a machine-learning context, it is assumed that a model developed on a particular dataset should perform the best when it is applied to that same dataset (Mod-PA approach). The datasets

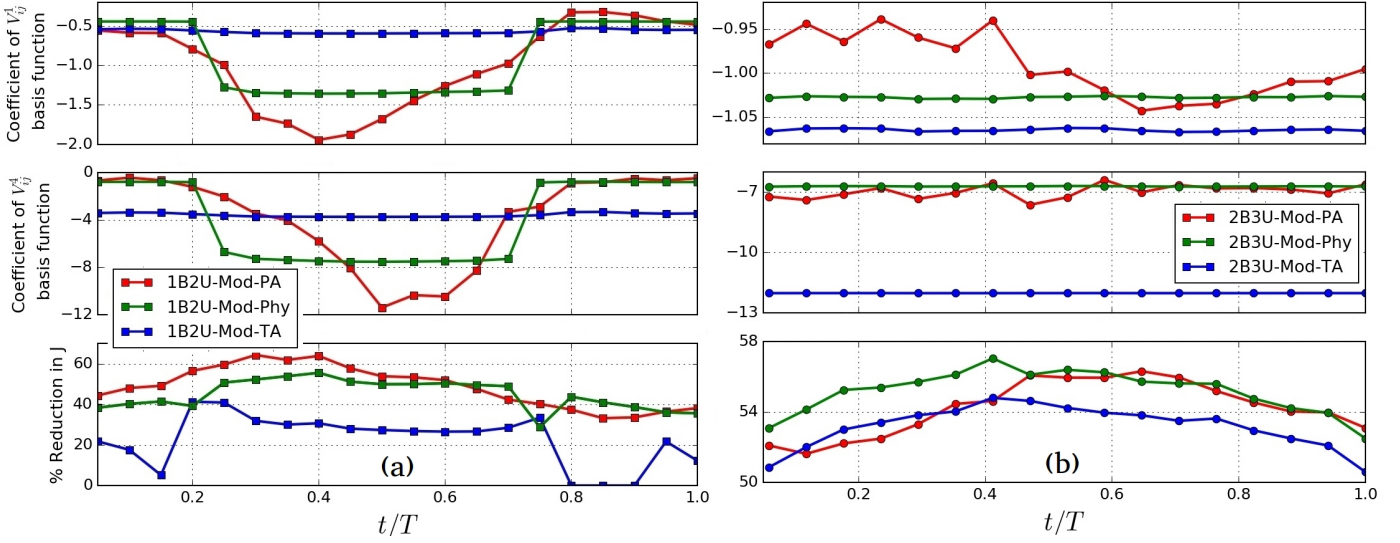


**Figure 11:** Coefficients of  $V_{ij}^1$  and  $V_{ij}^4$  basis functions and percentage reduction in normalized mean square error ( $J\%$ ) in the TE wake region of the (a) 1B2U & (b) 2B3U cases, when models developed using the Mod-PA, Mod-Phy and Mod-TA approaches are tested on phase-lock averaged data across one time period.

from the Mod-PA approach serve as test data for the models generated from the Mod-Phy and Mod-TA approaches. It is thus desirable to develop Mod-Phy & Mod-TA models that offer comparable performance to the Mod-PA models. For the TE wake region in the 1B2U case, based on the insights gained from Figs. 5(a), 6 and 7, two physics based models were created: one comprising data from phases 5-14 and the other comprising data from phases 1-4 & 15-20. For the 2B3U case, only one physics based models was created. Equations of the developed models using the Mod-Phy approach for the TE wake region for the 1B2U and 2B3U cases are presented below. Only the linear portion of the coefficients of the tensor basis function are provided:

1B2U-Mod-Phy: Phases 1-4 & 15-20:

$$a_{ij}^{EARSM} = -\frac{v_t}{k} S'_{ij} + (-0.448 + 0.094I_1 + 0.005I_2)V_{ij}^1 + (0.387 - 0.14I_1 + 0.947I_2 + 0.387)V_{ij}^2 + (1.036 - 0.758I_1 + 0.853I_2)V_{ij}^3 + (-0.87 + 1.6I_1 - 0.6I_2)V_{ij}^4. \quad (6)$$

1B2U-Mod-Phy: Phases 5-14:

$$a_{ij}^{EARSM} = -\frac{v_t}{k} S'_{ij} + (-1.39 + 12.648I_1 + 6.641I_2)V_{ij}^1 + (4.66 - 13.304I_1)V_{ij}^2 + (5.097 - 9.776I_1 + 10.476I_2)V_{ij}^3 + (-8 + 15.606I_1 - 48.9I_2)V_{ij}^4. \quad (7)$$

2B3U-Mod-Phy:

$$a_{ij}^{EARSM} = -\frac{v_t}{k} S'_{ij} + (-1.11 + 9.784I_1 + 2.613I_2)V_{ij}^1 + (-1.198 + 2.215I_1 + 16.066I_2)V_{ij}^2 + (5.8 - 22.575I_1 + 34.15I_2)V_{ij}^3 + (-7.608 + 40.486I_1 - 44.913I_2)V_{ij}^4. \quad (8)$$

Figure 11 represents the coefficients of the  $V_{ij}^1$  and  $V_{ij}^4$  basis functions in the TE wake region for the (a) 1B2U and (b) 2B3U

cases, when models developed using the Mod-PA, Mod-Phy and Mod-TA approaches are tested on each of the phase-lock averaged datasets. The percentage reduction in the normalized mean square error ( $J\%$ ) is also shown. In the 1B2U case, the 1B2U-Mod-TA model does not seem to predict the basis function coefficients accurately when compared to the models developed using the 1B2U-Mod-PA approach as the effect of the laminar separation bubbles is washed out due to the time averaging process. What remains in the time-average is just an attached boundary layer which offers an average additional diffusion coefficient of -0.57 and a  $V_{ij}^4$  coefficient of -3.9, which is quite different from the coefficients in phases 5-14 where laminar separation is seen. For certain phases, this model gives a negative reduction in the mean square error which can be attributed to the improper prediction of all the coefficients of the tensor basis functions. For the 2B3U case, the model 2B3U-Mod-TA offers much better performance than its corresponding 1B2U case, as there is a much smaller variance in the physics that is occurring between different phases. There is still, however, a neutralizing effect of certain flow physics in the time averaged flow field which results in the slight over prediction of the coefficients of some of the tensor basis functions. This accounts for the marginal difference in the normalized mean square error as compared to the models developed on individual phases (2B3U-Mod-PA).

In both the cases, the models that were developed using the Mod-Phy approach offer a good prediction of the coefficients of the basis functions, as there is similar percentage error reduction as compared to the Mod-PA approach. In the 1B2U case, the hypothesis of using 2 Mod-Phy (1B2U) models seems the correct way of approaching the problem, as it has captured the coefficients of the basis functions in phases 1-4 & 15-20 quite closely when compared with the coefficients obtained using the 1B2U-Mod-PA models. The value of the basis function coefficients for phases 5-14, derived via the Mod-Phy approach, appears like a weighted average value of the coefficients of

the tensor basis functions in phases 5-14 from the Mod-PA approach. At the junction where one model is switched on and the other switched off (phases 4 & 15, 1B2U case) there is a slight drop in the percentage mean square error reduction. This issue can be alleviated by using a combination of the two Mod-Phy models or a ramping function during run-time. This will either eliminate or alleviate the slope of the kink in the percentage error reduction plot around phases 4 & 15. The 2B3U-Mod-Phy model also performs equally well or slightly better when compared with the 2B3U-Mod-PA models, for the 2B3U case. From the perspective of model versatility, it has been observed that the 2B3U-Mod-Phy model, when applied to the TE wake region of phases 5-14 offers an average percentage error reduction ( $J\%$ ) of 37%, whereas the 1B2U-Mod-Phy model developed on phases 5-14, and tested on the TE wake region of the 2B3U case offers an average percentage error reduction ( $J\%$ ) of 45%. This shows that the models can be interchangeably used in regions of similar physics for different operating conditions.

## COMPARISON OF MODELS

The Mod-TA approach, in the context of cases with unsteady inflow conditions, have limited applicability for model development, as some of underlying phenomena related to deterministic unsteadiness is neutralized due to time averaging. As shown above, if there is a variance in the boundary layer physics, these models offer negative or zero improvement over the Boussinesq approximation, for some phases. It has been shown in earlier studies [28] that models trained only on the wake region rather than the wake and wake passages combined, offer larger improvements in the overall flow. Therefore, the Mod-TA approach cannot yield effective models for the incoming and intermediate wake regions (Fig. 3) as these wakes get washed out due to time averaging. They can however be used for the model development in the TE region for a case which has a high reduced frequency (i.e. presence of wake-fogging) with a good degree of reliability. Due to their limited applicability, these models have been excluded from the comparison study conducted in Fig. 12.

Mod-Phy models offer comparable, or in some cases slightly better performance not only for the TE wake regions, as discussed in detail in the previous section, but also for the incoming and intermediate wake regions, when compared with the Mod-PA approach for the respective region and case. For the incoming and intermediate wake regions of both cases, one Mod-Phy model is sufficient for each of the regions, as they produce an error reduction matrix qualitatively similar to Fig. 5(b). The formulation of the models using the Mod-Phy approach for the intermediate and incoming wake regions of the 2B3U case are quite similar, and as such one model can be used to enhance the anisotropy prediction across both of these regions. This, however, does not hold for the 1B2U case, as, due to the discrete nature of the wakes, different physics dominates in the incoming wake and intermediate wake regions. This implies that four and two Mod-Phy based models are required to enhance the wake mixing for the entire LPT domain of the 1B2U and 2B3U cases respectively.

It was also observed that Mod-Phy models developed on any of the wake regions of the 1B2U case (discrete wakes)

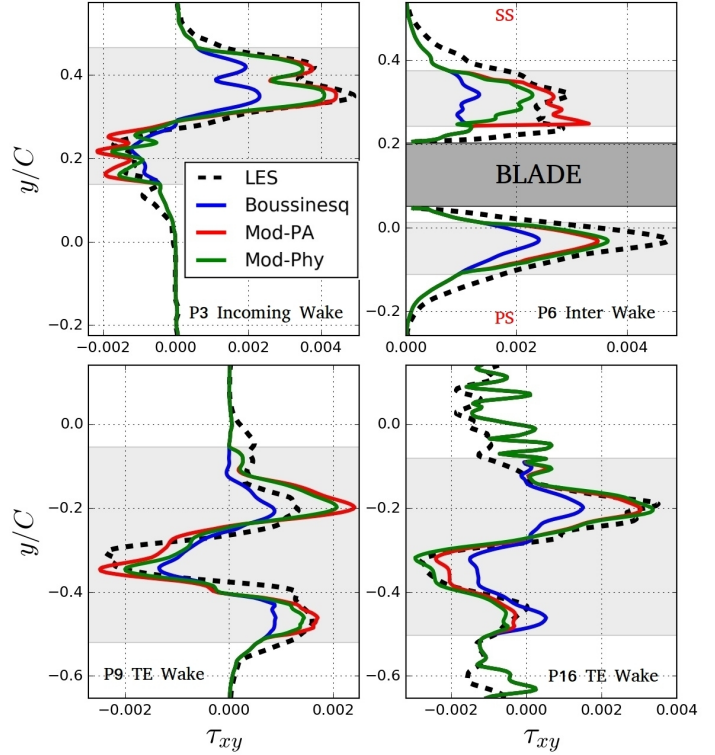


**Figure 12:** Reynolds shear stress profiles for selected locations (shown in Fig. 3) and phases across the three training regions for the 1B2U case.

when tested on the same regions of the 2B3U case (wake-fogging) perform better than the Mod-Phy models that were developed on any of the wake regions of the 2B3U case and tested on the same regions of the 1B2U case; which shows that models developed on cases with discrete wakes are more robust. It is anticipated that since the Mod-Phy models developed on the 1B2U case perform well on the 2B3U case, which has a largely different reduced frequency and flow coefficient, these should also perform well for cases with different (smaller range than 2B3U) reduced frequencies and flow coefficients, such as 1B1U, 1B3U and 2B1U cases [2], which are also of interest to the blade designer.

If the wake mixing prediction is to be enhanced, it is important that the prediction of the  $\tau_{xy}$  component of the Reynolds stress tensor is enhanced as compared to the Boussinesq approximation [38]. Using the eddy viscosity calculated via a least square optimized approach [27], shear stress profiles for the three wake regions (Fig. 3) and different phases (calculated based on LES data) have been shown in Fig. 12 for the 1B2U case. The shear stress profiles obtained via the LES data (reference), Boussinesq approximation, Mod-PA and Mod-Phy models (for the respective phase and region) are shown. The light grey region in these figures depicts where the EARSMs have been switched on. At other locations, the Boussinesq approximation is used. The locations where these profiles are extracted are shown by the dashed lines in Fig. 3. Figure 12(a) shows the  $\tau_{xy}$  profiles at 20% C upstream of the blade leading edge for phase 3. In this case, the Mod-Phy and Mod-PA models offer comparable performance with respect to one an-

other. These models bring about significant improvement in  $\tau_{xy}$  as compared to the Boussinesq approximation. Similar observations have been made for the intermediate wake region (Fig. 12(b)), which shows shear stress profiles along a vertical line 35% C downstream of the blade leading edge. However, in this case, the Mod-PA model in phase 6 does slightly better on the suction side of the intermediate wake than the Mod-Phy model. On the pressure side the performance of these two models is comparable.

In the TE wake region (profiles are extracted 20% C downstream of the blade TE), both the Mod-Phy models obtained are tested on the corresponding phases. Figure 12(c) shows the  $\tau_{xy}$  profile using the Mod-Phy model with higher additional diffusion (Eq. (7)), tested on phase 9. Overall, the Mod-Phy model performs quite well as compared to the Mod-PA model and brings about significant improvements in  $\tau_{xy}$  over the Boussinesq approximation. In phase 16 of the TE wake (Fig. 12(d)), the Mod-Phy model (Eq. (6)) traces out the LES stress profile quite accurately, and in fact performs better than the Mod-PA model developed on the TE wake of phase 16. These profiles consolidate the finding that the Mod-Phy models have the potential to offer a comparable, or at times, even slightly better performance as compared to a corresponding model that was developed using the individual phases (Mod-PA). Similar observations have also been made for other secondary statistics such as the other Reynolds stress components and TKE production, but are not shown here for the sake of brevity. Improvements in all these areas indicate that these models are enhancing the wake-mixing prediction to a high degree in the *a priori* sense, and thus have tremendous potential to improve the wake-mixing prediction when implemented into URANS calculations.

## CONCLUSIONS

This study explored methods to improve the URANS prediction of LPT wake-induced unsteady bladerow interactions, by creating a framework for the development of EARSMs using a machine learning approach. The models were developed using an LES database at an isentropic exit Reynolds number of 100,000 at two operating conditions. EARSMs were developed with the help of three distinct approaches namely, using individual phase-lock averaged data (Mod-PA), using data from a combination of phases with similar physics (Mod-Phy), and using the time averaged statistics (Mod-TA). It is however quite tedious for a designer to apply a number of Mod-PA type models in one simulation. Therefore, the Mod-Phy and Mod-TA approaches were proposed. Using phase-lock averaged data, a detailed analysis of the wake physics to aid EARSM development was conducted for the TE wake region. In the TE wake region of the 1B2U case (or broadly, low reduced frequencies), there were two distinctly prominent physical phenomena; one dominated by the Kelvin-Helmholtz roll-up vortices, which lead to larger additional turbulent diffusion in the boundary layer and the TE wake region, and the other was the presence of a calm boundary layer which lead to lower additional diffusion. Based on these two physical phenomena, two Mod-Phy based EARSMs were proposed to capture the physics more accurately for the TE wake region of the 1B2U case, and one Mod-Phy

based EARSM was proposed for the TE wake region of the 2B3U case. This analysis showed that the models developed via the Mod-Phy approach offer comparable, or at times, slightly better performance than the Mod-PA approach when tested on a number of different phases and regions. The Mod-Phy based EARSMs are not only robust when tested on different operating conditions than they were trained on, but also demonstrate significant improvements over the Boussinesq approximation in terms of the *a priori* analysis conducted, and thus have enhanced the wake-mixing prediction. Therefore, the Mod-Phy approach is deemed to be the most comprehensive approach for model development for cases with unsteady inflow conditions. The applicability of the Mod-TA approach is restricted to cases where there is wake-fogging. It was also found that the contribution of non-linear basis functions to the percentage error reduction rises as there is an increase in the intermediate wake to TE profile wake interaction. The immediate next step is to implement these models into URANS calculations to assess their performance over a wide range of operating conditions in order to further demonstrate their robustness.

## ACKNOWLEDGMENTS

This work was supported by the resources provided by the Pawsey Supercomputing Centre with funding from the Australian Government and the Government of Western Australia. The support by the Australian Government Research Training Program Scholarship is acknowledged. The University of Melbourne authors also acknowledge the financial support and the permission to publish by General Electric.

## REFERENCES

- [1] Schobeiri, M. T., and Ozturk, B., 2004. "Experimental Study of the Effect of Periodic Unsteady Wake Flow on Boundary Layer Development, Separation, and Re-attachment Along the Surface of a Low Pressure Turbine Blade". In ASME Turbo Expo, pp. GT2004-53929.
- [2] Michelassi, V., Chen, L., Pichler, R., Sandberg, R., and Bhaskaran, R., 2016. "High-Fidelity Simulations of Low-Pressure Turbines: Effect of Flow Coefficient and Reduced Frequency on Losses". *J. Turbomach.*, **138(11)**(November), p. 111006.
- [3] Arndt, N., 1993. "Blade Row Interaction in a Multistage Low-Pressure Turbine". *J. Turbomach.*, **115(1)**, p. 137.
- [4] Stieger, R. D., and Hodson, H. P., 2004. "The Transition Mechanism of Highly-Loaded LP Turbine Blades". *J. Turbomach.*, pp. 536–543.
- [5] Stieger, R. D., and Hodson, H. P., 2005. "The Unsteady Development of a Turbulent Wake Through a Downstream Low-Pressure Turbine Blade Passage". *J. Turbomach.*, **127(2)**, p. 388.
- [6] Halstead, D. E., Wisler, D. C., Okiishi, T. H., Walker, G. J., Hodson, H. P., and Shin, H. W., 1997. "Boundary Layer Development in Axial Compressors and Turbines : Part 3 of 4 - LP Turbines". *J. Turbomach.*, **119**(April), pp. 225–237.
- [7] Michelassi, V., Chen, L. W., Pichler, R., and Sandberg, R. D., 2015. "Compressible Direct Numerical Simulation of Low Pressure Turbine - Part II: Effect of Inflow Disturbances". *J. Turbomach.*, **137(7)**, p. 71005.
- [8] Ranjan, R., Deshpande, S. M., and Narasimha, R., 2017. "New Insights from High-Resolution Compressible DNS Studies on an LPT Blade Boundary Layer". *Comput. Fluids.*, **153**, pp. 49–60.
- [9] Wissink, J. G., 2003. "DNS of Separating, Low Reynolds Number Flow in a Turbine Cascade with Incoming Wakes". *Int. J. Heat Fluid Flow.*, **24(4)**, pp. 626–635.
- [10] Michelassi, V., Wissink, J. G., and Rodi, W., 2003. "Direct Numerical Simulation, Large Eddy Simulation and Unsteady Reynolds-Averaged NavierStokes Simulations of Periodic Unsteady Flow in a Low-Pressure

- Turbine Cascade: A Comparison". *Proc. Inst. Mech. Eng. Part A J. Power Energy*, **217**(4), pp. 403–411.
- [11] Praisner, T. J., Clark, J. P., Nash, T. C., Rice, M. J., and Grover, E. A., 2006. "Performance Impacts Due to Wake Mixing in Axial Flow Turbomachinery". In ASME Turbo Expo, no. GT2006-90666.
- [12] Keadle, K., and McQuilling, M., 2013. "Evaluation of RANS Transition Modeling for High Lift LPT Flows at Low Reynolds Number". In Proc. ASME Turbo Expo 2013 Turbine Tech. Conf. Expo., pp. GT2013-95069.
- [13] Pacciani, R., Marconcini, M., Arnone, A., and Bertini, F., 2013. "Predicting High-Lift Low-Pressure Turbine Cascades Flow Using Transition-Sensitive Turbulence Closures". *J. Turbomach.*, **136**(5), p. 051007.
- [14] Schmitt, G., 2007. "About Boussinesq's Turbulent Viscosity Hypothesis: Historical Remarks and a Direct Evaluation of its Validity.". *Comptes Rendus Mec. Elsevier Masson*, **335**(9), pp. 617–627.
- [15] Pope, S. B., 1975. "A More General Effective-Viscosity Hypothesis". *J. Fluid Mech.*, **72**(2), pp. 331–340.
- [16] Gatski, T., and Speziale, C., 1993. "On Explicit Algebraic Stress Models for Complex Turbulent Flows". *J. Fluid Mech.*, **254**, pp. 59–78.
- [17] Wallin, S., and Johansson, A. V., 2000. "An Explicit Algebraic Reynolds Stress Model for Incompressible and Compressible Turbulent Flows". *J. Fluid Mech.*, **403**, pp. 89–132.
- [18] Duraisamy, K., Zhang, Z. J., and Singh, A. P., 2015. "New Approaches in Turbulence and Transition Modeling Using Data-driven Techniques". *53rd AIAA Aerosp. Sci. Meet.*, **I284**.
- [19] Singh, A. P., Medida, S., and Duraisamy, K., 2017. "Machine-Learning-Augmented Predictive Modeling of Turbulent Separated Flows over Airfoils". *AIAA J.*, **55**(7), pp. 2215–2227.
- [20] Ling, J., Kurzawski, A., and Templeton, J., 2016. "Reynolds Averaged Turbulence Modelling Using Deep Neural Networks with Embedded Invariance". *J. Fluid Mech.*, **807**(2016), pp. 155–166.
- [21] Wang, J.-X., Wu, J.-L., and Xiao, H., 2017. "A Physics Informed Machine Learning Approach for Reconstructing Reynolds Stress Modeling Discrepancies Based on DNS Data". *Phys. Rev. Fluids*, **2**(3), p. 034603.
- [22] Wu, J.-L., Xiao, H., and Paterson, E., 2018. "Physics-Informed Machine Learning Approach for Augmenting Turbulence Models: A Comprehensive Framework". *Phys. Rev. Fluids*, **3**(July), p. 074602.
- [23] Milani, P. M., Ling, J., and Eaton, J. K., 2018. "Physical Interpretation of Machine Learning Models Applied to Film Cooling Flows". In ASME Turbo Expo, pp. GT2018–76927.
- [24] Ferreira, C., 2001. "Gene Expression Programming: a New Adaptive Algorithm for Solving Problems". *Complex Syst.*, **13**(2), pp. 87–129.
- [25] Weatheritt, J., and Sandberg, R. D., 2016. "A Novel Evolutionary Algorithm Applied to Algebraic Modifications of the RANS Stress-Strain Relationship". *J. Comput. Phys.*, **325**, pp. 22–37.
- [26] Weatheritt, J., and Sandberg, R. D., 2017. "The development of algebraic stress models using a novel evolutionary algorithm". *Int. J. Heat Fluid Flow*, **68**(September), pp. 298–318.
- [27] Weatheritt, J., Pichler, R., Sandberg, R. D., Laskowski, G., and Michelassi, V., 2017. "Machine Learning for Turbulence Model Development Using a High Fidelity HPT Cascade Simulation". In ASME Turbo Expo 2017 Turbomach. Tech. Conf. Expo., pp. GT2017—63497.
- [28] Akolekar, H. D., Weatheritt, J., Hutchins, N., Sandberg, R. D., Laskowski, G., and Michelassi, V., 2018. "Development and Use of Machine-Learnt Algebraic Reynolds Stress Models for Enhanced Prediction of Wake Mixing in LPTs". In ASME Turbo Expo 2018 Turbomach. Tech. Conf. Expo., pp. GT2018–75447.
- [29] Sandberg, R., Tan, R., Weatheritt, J., Ooi, A., Haghiri, A., Michelassi, V., and Laskowski, G., 2018. "Applying Machine Learnt Explicit Algebraic Stress and Scalar Flux Models To a Fundamental Trailing Edge Slot". In ASME Turbo Expo, pp. GT2018–75444.
- [30] Rodi, W., 1976. "A New Algebraic Relation for Calculating the Reynolds Stresses". In Gesellschaft Angew. Math. und Mech. Work. Paris Fr., Vol. 56.
- [31] Stadtmüller, P., and Fottner, L., 2001. "A Test Case for the Numerical Investigation of Wake Passing Effects on a Highly Loaded LP Turbine Cascade Blade". *ASME Turbo Expo*, pp. GT–2001–0311.
- [32] Lopez, M., and Walters, D. K., 2016. "Prediction of Transitional and Fully Turbulent Flow Using an Alternative to the Laminar Kinetic Energy Approach". *J. Turbul.*, **17**(3), pp. 253–273.
- [33] Parneix, S., Laurence, D., and Durbin, P. A., 1998. "A Procedure for Using DNS Databases". *J. Fluids Eng. Trans. ASME*, **120**(1), pp. 40–46.
- [34] Lumley, J. L., 1970. "Toward a turbulent constitutive relation". *J. Fluid Mech.*, **41**(2), pp. 413–434.
- [35] Michelassi, V., and Wissink, J. G., 2015. "Turbulent Kinetic Energy Production in the Vane of a Low-Pressure Linear Turbine Cascade with Incoming Wakes". *Int. J. Rotating Mach.*, **2015**, p. 650783.
- [36] Hatman, A., and Wang, T., 1998. "Separated-Flow Transition: Part I - Experimental Methodology and Mode Classification". In Int. Gas Turbine Aeroengine Congr. Exhib. Stock. Sweden.
- [37] Hodson, H. P., and Howell, R. J., 2005. "Bladerow Interactions, Transition, and High-Lift Aerofoils in Low-Pressure Turbines". *Annu. Rev. Fluid Mech.*, **37**(1), pp. 71–98.
- [38] Leschziner, M., 2015. *Statistical Turbulence Modelling for Fluid Dynamics - Demystified: an Introductory Text for Graduate Engineering Students*. World Scientific.